Resonances in Symmetric and Asymmetric Semiconductor Laser Structures.

V.N. Stavrou[a,b], G.P. Veropoulos[a] and A. Markopoulos[a]

[a]*Division of Academic Studies, Hellenic Navy Petty Officers Academy, Skaramagkas, T.K. 12400, Greece*

[b]*Department of Physics and Astronomy, University of Iowa, Iowa City, IA 52242, USA*

Abstract. We have theoretically and numerically investigated the symmetric and asymmetric quantum well (QW) laser structures. Semiconductor structures made with symmetric QW (e.g. ZnSe/CdSe) and asymmetric QW (e.g. ZnS/ZnSe/CdSe) have been used several times due to their ability of lasing emission in the blue region of the electromagnetic spectrum. We have investigated the above mentioned QWs structures which are confined between metallic barriers in order to discretize the electron states with energies larger than the depth of the well. The phonon modes are described by the bulk phonon approximation and the DC model. In these structures, electron resonances appear when electrons drop to energies smaller than the depth of the well. In addition, further results are provided for another type of resonances named phonon resonance which emerges when the electron energy difference becomes equal to phonon mode energy. The two different phonon models predict almost the same scattering magnitude but the resonances appear at different well widths. Lastly, in contrast to the symmetric QWs, the asymmetric QWs cause smooth scattering rates close to resonance and antiresonance values.

Keywords: QW Laser structures, DC phonons, Bulk phonon approximation, scattering rates, II-VI's semiconductors.
PACS: 63.20.Dj, 72.10.Di, 72.20.Jv

INTRODUCTION

The use of II-VI compounds has been motivated by the possibility of generating quantum well lasers in the visible region of the electromagnetic spectrum. However, until recently, material properties have limited the performance of devices, but the significant improvements in the doping of these materials have made the possibility of optimum device performance better than before. Akira [1] announced that Sony were able to design a II-VI laser that operated for more than 100 hours [2]. The indication of a great device performance is therefore stronger and research towards a fuller exploitation of II-VI semiconductor quantum wells [3] will continue. A theoretical study of electron-phonon interactions in these quantum wells is therefore timely.

More significantly, a study of the characteristic process of capture of electrons into II-VI quantum wells would be useful.

Electron-phonon interactions in such an asymmetric II-VI heterostructure can fortunately be studied using continuum models and bulk phonon approximation for optical phonons [4] and the effective mass approximation for electrons. Studies of electron-phonon interaction in III-V heterostructure have led to the conclusion that, concerning the total transition rate by emission of optical phonons, the dielectric continuum (DC) and bulk phonon approximation model [4-8] are adequate for the evaluation of such rates using the Fermi golden rule. For studies of processes involving individual optical phonons, such as Raman scattering, the DC model should not be used and a description of the modes using the hybrid model [9] would be appropriate. Since our aim is to calculate total rates, we can use the DC and bulk phonons despite their shortcomings in Raman processes.

ELECTRONS AND PHONONS IN ASYMMETRIC QWS.

Let us consider the semiconductor heterostructure made with ZnS/ZnSe/CdSe, as it is illustrated in Figure 1. The size of the QW is L with barrier size D and the total structure size is L+2D. Using the boundary conditions [4-5] a) continuity of the electron wavefunctions (Ψ), b) continuity of $\frac{1}{m^*}\frac{d\Psi}{dz}$ at the interfaces ($z = 0 \text{ and } z = L$) and c) the vanishing of the wavefunctions at the metallic barriers ($z = -D \text{ and } z = D + L$) [9-11], the electron dispersion relations for the initial and final electron states are respectively given by

$$\tan(k_1 L) = \frac{b + a\cot(k_2 D)\tanh(k_3 D)}{\tanh(k_3 D) - ab\cot(k_2 D)}, \quad with\ V_2 < E(k_{\|} = 0) < V_3 \tag{1}$$

$$\tan(k_1 L) = \frac{b + a\coth(k_2 D)\tanh(k_3 D)}{\tanh(k_3 D) - ab\coth(k_2 D)}, \quad with\ E(k_{\|} = 0) < V_2$$

where $a = \frac{k_2 m_1^*}{k_1 m_2^*}$ and $b = \frac{k_3 m_1^*}{k_1 m_3^*}$. The effective masses m_i^* and the electron wavevectors k_i ($i = 1,2,3$) correspond to each region as presented in Figure 1.

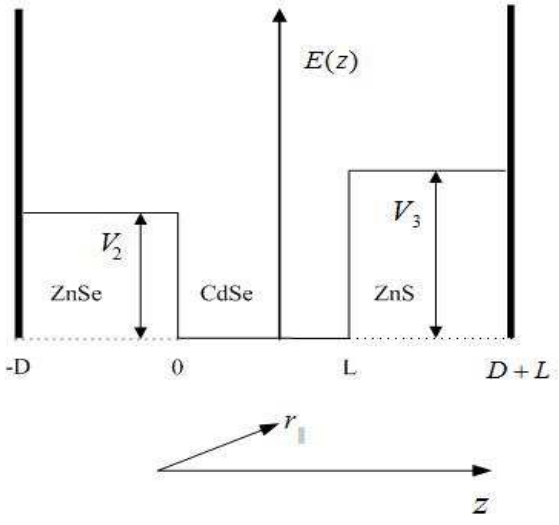

FIGURE 1. A typical asymmetric QW heterostructure with metallic barriers at $-D$ and $D+L$.

The relative ionic displacement field vector $\mathbf{u}(\mathbf{r},\mathrm{t})$ is defined as the displacement of the positive ions relative to the negative ions multiplied by the square root of the reduced mass per unit volume [6]. The reduced mass of the positive and negative ions is defined by $\overline{\mathrm{M}} = \mathrm{M}_{+}\mathrm{M}_{-}/(\mathrm{M}_{+}+\mathrm{M}_{-})$. The displacement is coupled to the electric field $\mathbf{E}$ and paralization field $\mathbf{P}$ by the equations

$$\begin{aligned} \ddot{\mathbf{u}}(\mathbf{r},\mathrm{t}) &= \mathrm{b}_{11}\mathbf{u} + \mathrm{b}_{12}\mathbf{E} \\ \mathbf{P} &= \mathrm{b}_{12}\mathbf{u} + \mathrm{b}_{22}\mathbf{E} \end{aligned} \tag{2}$$

where the coefficients are defined by

$$\begin{aligned} b_{11} &= -\omega_T^2 \\ b_{12} = b_{21} &= \left[\varepsilon_0(\varepsilon_s - \varepsilon_\infty)\right]^{\frac{1}{2}}\omega_T \\ b_{22} &= \varepsilon_0(\varepsilon_\infty - 1) \end{aligned} \tag{3}$$

Below, we introduce the theoretical frame for the bulk phonon approximation and DC model which are used to describe the longitudinal optical phonons (LO). The above mentioned phonon models are based on the Born and Huang theory (eq. 2).

The bulk phonon approximation considers that there is only one phonon mode which propagates with the LO frequency of the well material. The quantized bulk LO phonons are described by the scalar quantised field

$$\hat{\Phi}(\mathbf{r},\mathrm{t}) = -\int \mathrm{d}^3\mathbf{q}\frac{\mathrm{i}}{|\mathrm{q}|}\left[\frac{\hbar\omega}{2\varepsilon_0(2\pi)^3}\left(\frac{1}{\varepsilon_\infty}-\frac{1}{\varepsilon_\mathrm{s}}\right)\right]^{\frac{1}{2}}\left(\mathrm{e}^{\mathrm{i}(\mathbf{q}\cdot\mathbf{r}-\omega\mathrm{t})}a_\mathrm{q} + \mathrm{H.C.}\right) \tag{4}$$

where H.C. stands for “Hermitian conjugate”.

The DC model makes use of the theoretical framework given by Born and Huang as earlier described. The DC model consists of the following two types of phonons: a) confined modes and b) interface (IP) modes. The model assumes the existence of the dielectric function $\varepsilon(\omega)$ for each material. However, it states quasistate limit for the outset. The field is therefore also described by a scalar potential Φ (eq. 4) and, because of the absence of spatial dispersion, the boundary conditions applicable to the layer interfaces are only electromagnetic boundary conditions. Since all adjacent materials in the asymmetric quantum well are different, the values of ω_{Li} are different. This means that oscillations of frequency ω_{Li} in material i cannot be sustained by the adjacent material (confined modes). It follows that the oscillations for the confined modes must vanish at the boundary for each material. We therefore set Φ to be zero at all boundaries.

$$\Phi(\mathbf{r}_\parallel, z, t) = \sum_j \int d^2\mathbf{q}_\parallel \left(\phi_j(z)e^{i(\mathbf{q}_\parallel\cdot\mathbf{r}_\parallel - \omega_j(\mathbf{q}_\parallel)t)}\ a(\mathbf{q}_\parallel, j) + H.C.\ \right) \tag{5}$$

For the IP modes, at the interfaces Φ also has to be continuous at $z=0$, $z=L$ and its derivative with respect to z multiplied by the dielectric function should be continuous at these interfaces. It is worth mentioning that the IP modes have potential maxima at the QW region and

should vanish at the outer interfaces. As a result, the dispersion relation for the IP modes [10] is given by

$$\frac{\varepsilon_1(\varepsilon_2+\varepsilon_3)}{\varepsilon_1^2\tanh(q_{\parallel}D)+\varepsilon_2\varepsilon_3\coth(q_{\parallel}D)} = -\tanh(q_{\parallel}L) \tag{6}$$

In the case in which materials 2 and 3 are the same, the dispersion relation gets the corresponding IP dispersion of the symmetric QWs with metallic barriers [11].

SCATTERING MECHANISM AND CONCLUSIONS

In this section, we have studied the quantum capture mechanism. The total capture rate is the sum of the transition rates for the initial state to all possible bound states by emission of one of the possible polar optical modes. If $|\mathbf{k}_{\parallel}^{i}\rangle$ is an initial quantum well electronic state, $|\mathbf{k}_{\parallel}^{f}\rangle$ one of the possible final states and $|\{\mathbf{q}_{\parallel}, j\}\rangle$ a possible polar mode state with one quantum, then the total transition rate for all possible branches j is given by:

$$\Gamma_{total} = \sum_{j=1}^{N}\Gamma_j \tag{7}$$

where Γ_j is the contribution due to polar branch j. The rates are calculated using the Fermi golden rule (assuming that only emission is possible)

$$\Gamma_j(\mathbf{k}_{\parallel}^{i}) = \frac{2\pi}{\hbar}\int d^2\mathbf{k}_{\parallel}^{f}\int d^2\mathbf{q}_{\parallel}\left|<\mathbf{k}_{\parallel}^{i};0\,|\,e\Phi\,|\,\mathbf{k}_{\parallel}^{f};\{\mathbf{q}_{\parallel}, j\}>\right|^2\delta(\mathrm{E}_i-\mathrm{E}_f-\hbar\omega_j(\mathbf{q}_{\parallel})) \tag{8}$$

In the above equation, E_i and E_f stand for electronic energy initial and final state respectively. $\mathbf{k}_{\parallel}^{i}$ and $\mathbf{k}_{\parallel}^{f}$ are the wave vectors for the initial and final state respectively and $\omega_j(\mathbf{q}_{\parallel})$ is the mode frequency of the emitted polar mode of branch j. The interaction Hamiltonian which couples the electrons to the polar optical modes is given by

$$\begin{aligned} H_{\mathrm{int}} &= e\Phi(\mathbf{r}_{\parallel}, z, t) \\ &= e\sum_j\int d^2\mathbf{q}_{\parallel}\left(\phi_j(z)e^{i(\mathbf{q}_{\parallel}\cdot\mathbf{r}_{\parallel}-\omega(\mathbf{q}_{\parallel},j)t)}+H.C.\right) \end{aligned} \tag{9}$$

where e is the electronic charge.

Figure 2 shows the total bulk-phonon-mediated and the DC-phonon-mediated capture rate against L calculated for the electrons at the bottom of the first subband above the well which drop in all possible states within the QW. The capture rates are evaluated by the eq. 7 using numerical integration techniques (e.g. Monte Carlo integration). The rate shows regular peaks with an overall approximately linear increase as L increases. The peaks are associated with two distinct physical characteristics of the system: the onset of electron resonances and the threshold emission of phonons. The electron resonances are distinguished by a sharp drop, while the phonon peaks have sudden thresholds as L increases. The electron resonances arise when the initial subband enters the well which occurs at regular intervals of L [9-11]. At these

points the highest probability distribution of the electrons shifts from the barrier regions to the well, thus increasing the overlap integrals in the matrix elements between this state and the states already in the well. Since the scattering into each subband is about the same for any L at an electron resonance, the rate is proportional to the number of subbands in the well. Hence, the height of the electron resonance peaks increases linearly with QW width. The sudden drop occurs because the new initial subband is higher in energy and one of the characteristics of this state is that the highest electron probability is in the barriers; the matrix elements decrease and so does the total capture rate. The other set of peaks is due to the possibility of scattering into a new subband by emitting phonons. This threshold appears for a larger QW width than each electron resonance and occurs when the previous initial state is in the well and also when the energy conservation requirements with $q_{\|} = 0$ are met. This gives a sudden increase but only depends on the scattering into one subband which decreases as the energy difference between the initial and the final subband increases with increasing well width. These peaks also have approximately the same height because not all subbands in the well but only one subband is involved. These are also generally smaller than the electron resonance peaks because the overlap integral is highest in the barrier regions leading to smaller transition matrix elements.

The electron capture rates via the emission of bulk phonons have the same electron resonance magnitude due to the fact that the electron resonance is independent of the phonon model. The positions (well widths) where the phonon resonances appear and the size of the peaks are different for DC and bulk phonons because of the different phonon frequencies which are predicted by different models.

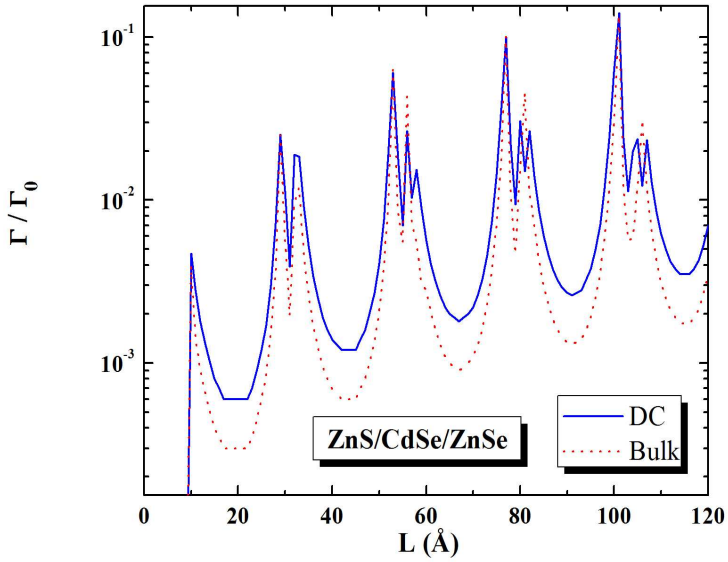

FIGURE 2. The electron capture rates for an asymmetric QW (with $D = 200$ $\overset{0}{A}$).

Lastly, Figure 3 illustrates the electron capture rates in the case of the symmetric QW made with CdSe/ZnSe (II-VI semiconductor compounds) assisted by DC and Bulk phonons. Resonance peaks emerge in regular intervals because of the earlier mentioned conditions which give rise to electron and phonon resonances. As it is obvious, the asymmetry of the structure does not allow the antiresonances to be very sharp as in the case of the symmetric QW. Furthermore, concerning the antiresonance magnitude between the symmetric and asymmetric

heterostructures, the order of magnitude difference is either one or two and the resonances for the case of asymmetric QW are larger than for the case of the symmetric QW.

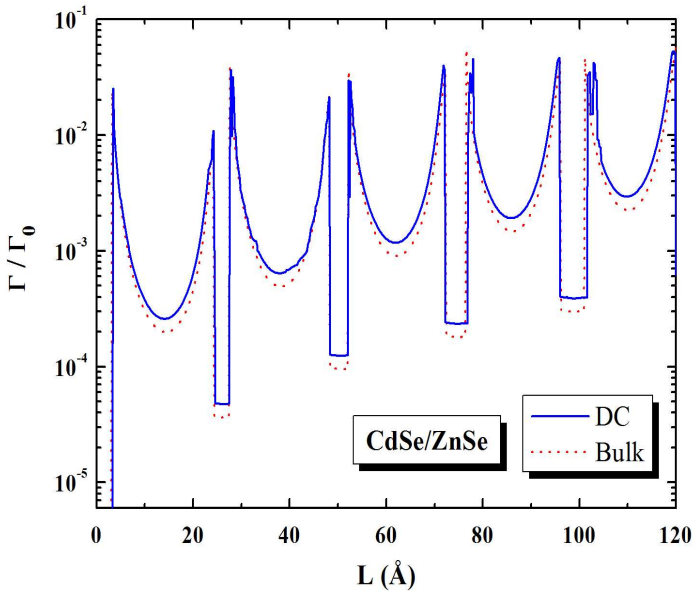

FIGURE 3. The electron capture rates for a symmetric QW (with $D = 200\ \overset{0}{A}$).

Summing over all, we have theoretically and numerically investigated the electron capture mechanism by considering only emission of LO phonons. The electron capture rates assisted by the DC and bulk phonons are in a very good agreement (Figure 2 &3). Furthermore, the asymmetry of the heterostructure and the use of II-VI semiconductor compounds could be important parameters for both controlling the electron capture mechanism and studying semiconductor lasers which can operate in short wavelength regime of the electromagnetic spectrum [3] (e.g. blue-green region).

ACKNOWLEDGMENTS

The authors would like to thank Prof. M. Babiker, Prof. B.K. Ridley for useful discussions and Lt. Commander of the Hellenic Navy D. Filinis for his support. The author V.N.S. would like also to acknowledge the financial support given by the Training Mobility of Researchers (TMR), NSA and ARDA under ARO Contract No. DAAD19-03-1-0128. and the University of Iowa under the grand No. 52570034.

REFERENCES

1. I. Akira, International II-VI conference, Edinburgh 1995 (III-V's Review Vol.**9**, No.**1**, page 66, 1996).
2. W. Meredith, III-V's Review, Vol.**9**, No.**3**, page 56, June 1996.
3. W.P. Risk, T.R. Gosnell and A.V. Nurmikko "Compact Blue-Green Lasers" (Cambridge University Press, 2003); Agrawal G. "Semiconductor lasers, past, present and future" (AIP Press, 1995).
4. Ridley B. K. 1982 "Quantum Processes in Semiconductors" 2nd edn (Oxford University Press).

5. Bastard G. 1992 “Wave mechanics applied to semiconductor heterostructure” (Wiley-Interscience).
6. Born M. and Huang K. 1968 Dynamic Theory of Crystal Lattices (Oxford : Clarendon).
7. Fuchs R. and Kliewer K. L., Phys. Rev. **140A**, 2076 (1965).
8. Kliewer K.L. and Fuchs R. Phys. Rev. **144,** 495 (1966).
9. V.N. Stavrou, C.R. Bennett, O.M.M. Al-Dossary and M. Babiker, Phys. Rev. B **63**, 205304 (2001).
10. V.N. Stavrou, M. Babiker and C.R. Bennett, J. Phys.: Condens. Matter **13** (2001) 6489-6498.
11. V.N. Stavrou, C.R. Bennett, M. Babiker, N.A. Zakhleniuk and B. K. Ridley, Phys Low-Dimens. Str., **1-2** (1998) 23-32; V.N. Stavrou and G.P Veropoulos, Semicond. Sci. Technol., 2009, **24**(9) 095014.